

RESEARCH ARTICLE

10.1002/2013JA019697

Key Points:

- Substantial structures are present in Mars's ionospheric plasma
- These are likely related to Mars's highly varied crustal fields
- We show that these structures are very stable phenomena

Correspondence to:

D. J. Andrews,
david.andrews@irfu.se

Citation:

Andrews, D. J., M. André, H. J. Opgenoorth, N. J. T. Edberg, C. Diéval, F. Duru, D. A. Gurnett, D. Morgan, and O. Witasse (2014), Oblique reflections in the Mars Express MARSIS data set: Stable density structures in the Martian ionosphere, *J. Geophys. Res. Space Physics*, 119, doi:10.1002/2013JA019697.

Received 6 DEC 2013

Accepted 13 APR 2014

Accepted article online 17 APR 2014

Oblique reflections in the Mars Express MARSIS data set: Stable density structures in the Martian ionosphere

D. J. Andrews¹, M. André¹, H. J. Opgenoorth¹, N. J. T. Edberg¹, C. Diéval², F. Duru², D. A. Gurnett², D. Morgan², and O. Witasse³

¹Swedish Institute of Space Physics, Uppsala, Sweden, ²Department of Astronomy, University of Iowa, Iowa City, Iowa, USA, ³ESA ESTEC, Noordwijk, Netherlands

Abstract The Mars Advanced Radar for Subsurface and Ionospheric Sounding (MARSIS) onboard the European Space Agency's Mars Express (MEX) spacecraft routinely detects evidence of localized plasma density structures in the Martian dayside ionosphere. Such structures, likely taking the form of spatially extended elevations in the plasma density at a given altitude, give rise to oblique reflections in the Active Ionospheric Sounding data. These structures are likely related to the highly varied Martian crustal magnetic field. In this study we use the polar orbit of MEX to investigate the repeatability of the ionospheric structures producing these anomalous reflections, examining data taken in sequences of multiple orbits which pass over the same regions of the Martian surface under similar solar illuminations, within intervals lasting tens of days. Presenting three such examples, or case studies, we show for the first time that these oblique reflections are often incredibly stable, indicating that the underlying ionospheric structures are reliably reformed in the same locations and with qualitatively similar parameters. The visibility, or lack thereof, of a given oblique reflection on a single orbit can generally be attributed to variations in the crustal field within the ionosphere along the spacecraft trajectory. We show that, within these examples, oblique reflections are generally detected whenever the spacecraft passes over regions of intense near-radial crustal magnetic fields (i.e., with a “cusp-like” configuration). The apparent stability of these structures is an important feature that must be accounted for in models of their origin.

1. Introduction

Like all planets with atmospheres, Mars possesses an ionosphere formed principally through solar photo-ionization [see, e.g., *Nagy et al.*, 2004; *Witasse et al.*, 2008; *Haider et al.*, 2011]. At Mars, this conductive medium provides a permanent obstacle to the impinging solar wind on the dayside, forming the planet's so-called “induced magnetosphere.” Mars lacks a large-scale (low-order) magnetic field, though it does possess extensive sources of magnetic fields embedded in a thin layer of crustal material. In locations such as Terra Sirenum, this crustal field is of sufficient strength to dominate that of the typical draped interplanetary magnetic field (IMF), and thereby significantly influence plasma processes in the ionosphere [e.g., *Withers et al.*, 2005; *Nielsen et al.*, 2007a]. Elsewhere, it is sufficiently weak that the magnetic field at ionospheric altitudes is controlled almost exclusively by the IMF strength and orientation. Such weak fields are largely confined to the Tharsis and Utopia regions in the northern hemisphere. Nevertheless, over a significant fraction of the planet's surface, the crustal field is of sufficient strength to readily influence the effects of electron precipitation [e.g., *Lillis et al.*, 2004; *Soobiah et al.*, 2006; *Brain et al.*, 2007].

Our understanding of the Martian ionosphere and induced magnetosphere has been significantly furthered by two recent successful orbiter missions, namely NASA's Mars Global Surveyor (MGS) and European Space Agency's (ESA's) Mars Express (MEX). The Mars Advanced Radar for Subsurface and Ionospheric Sounding (MARSIS) onboard MEX is a unique instrument in planetary exploration, comprising both a subsurface radar sounder (SS) and an Active Ionospheric Sounding (AIS)—a spaceborne ionosonde or topside sounder [*Picardi et al.*, 2004; *Gurnett et al.*, 2005]. The MARSIS hardware consists of two antennas: a 40 m tip-to-dip dipole and a shorter orthogonal monopole. The monopole antenna is used in SS sounding to provide a mechanism to reduce the influence of surface reflections received from off-nadir directions (known as “clutter” in radar parlance). However, the monopole is not used when MARSIS is used in the AIS mode. During AIS mode soundings, a 91.4 μ s duration pulse of central frequency f_s is transmitted on the dipole, and any specularly reflected signals received at the same frequency are then accumulated in 80 distinct 91.4 μ s delay intervals.

These reflections originate from those regions of the ionosphere in which the ionospheric plasma density n_e is such that the group velocity of the pulse goes to zero, i.e.,

$$n_e = \epsilon_0 m_e \left(\frac{2\pi f_s}{e} \right)^2 \approx f_s^2 \cdot 1.24 \times 10^{-8} \text{ cm}^{-3} \text{ Hz}^{-2}, \quad (1)$$

where n_e is expressed in units of cm^{-3} and f_s is in Hz (other symbols having their usual meanings [cf. Budden, 1961]). This process is subsequently repeated at 160 quasi logarithmically spaced values of f_s from ~ 0.1 to 5.5 MHz. Each frequency sweep generates an “ionogram,” being a 2-D plot of reflected intensity as a function of both delay time and sounding frequency. The maximum operating range of the radar, ~ 1100 km, is determined by the maximum delay recorded before transmission of a new sounding pulse. Owing to the specular nature of the reflection, return signals will only be received from those regions of the ionosphere in which surfaces of constant plasma density are normal to the raypath. Assuming a horizontally stratified ionosphere, specular reflections will be received with increasing delays at frequencies increasing from that of the local plasma medium surrounding the spacecraft f_{p0} up to the so-called “critical frequency” f_{pc} corresponding through equation (1) to the ionospheric peak density. The delay between transmission of a pulse and the reception of a reflection can be converted to an apparent distance assuming constant velocity propagation of the sounding pulse to and from the reflection site at the speed of light. However, this remains only an approximation due to the slowed propagation of the pulse through the intervening plasma and construction of plasma density profiles as a function of “true” altitude requires a numerical inversion scheme to be used [see, e.g., Budden, 1961; Gurnett et al., 2005; Sánchez-Cano et al., 2012; Morgan et al., 2013].

As the monopole is not used in AIS-mode soundings, in addition to the “principal” ionospheric reflection received along the nadir direction from the horizontally stratified ionosphere directly subspacecraft, additional reflections are frequently detected at oblique incidence. These so-called “oblique reflections,” initially reported by Gurnett et al. [2005], were further studied by Duru et al. [2006] and Nielsen et al. [2007b]. While these are typically dayside phenomena, somewhat similar (and likely related) anomalous reflections are also intermittently detected on the nightside from localized tenuous patches of plasma [Němec et al., 2010, 2011]. When the reflected signal at a single sounding frequency from multiple successive soundings taken along the spacecraft orbit is plotted in an apparent altitude versus time diagram, the principal ionospheric reflection appears at approximately constant apparent altitudes (except close to the terminator). Meanwhile, any oblique reflections present are generally evident as quasi-hyperbolic traces [Gurnett et al., 2005; Duru et al., 2006]. An example of the appearance of these oblique reflections is shown in Figure 1, in which we adopt a presentation format similar to that used previously, e.g., by Gurnett et al. [2005] and Duru et al. [2006]. These data were taken on MEX orbit 3286 on 31 July 2006. In Figure 1a, the intensity of the reflections received at the spacecraft in response to a sounding pulse at $f_s = 1.9$ MHz is shown color coded versus apparent altitude and time. Similar plots can be produced for all sounding frequencies transmitted, though distortions produced by the sounder in the vicinity of the spacecraft often obscure the majority of reflections at frequencies $f_s < 1.0$ MHz. The principal reflection is seen at a near-constant apparent altitude of ~ 100 km and is produced by specular reflections from ionospheric regions in which the local plasma is horizontally stratified with a density n_e of approximately $0.4 \times 10^5 \text{ cm}^{-3}$ (cf. equation (1)). Based on various models of the Martian ionosphere [Morgan et al., 2008; Němec et al., 2010; Sánchez-Cano et al., 2013], at these solar zenith angles, the $n_e = 0.4 \times 10^5 \text{ cm}^{-3}$ surface is expected to lie at an altitude of ~ 170 km. The difference between the “true” and apparent altitudes, introduced by the dispersion of the sounding pulse as it propagates through the ionosphere to its reflection point, is therefore ~ 60 km. Several distinct oblique reflections can be seen in Figure 1 in addition to the horizontal principal reflection. Each has a quasi-hyperbolic trace in apparent altitude and time, rising up to the apparent altitude of the principal reflection before falling once again, indicating the changing distance to the source of the oblique reflection as the spacecraft moves relative to it. In Figure 1b we show the magnitude $|\mathbf{B}|$ (black line) and radial component $|B_r|$ (red line) of the Lillis et al. [2010] Martian crustal magnetic field model, as evaluated at 150 km altitude along the MEX trajectory. Intervals of negative sign of the B_r component are indicated by a dashed line style. Figure 1c then shows the inclination angle δ of the magnetic field to the horizontal, where the line is shown dashed when $|\mathbf{B}| < 50$ nT. Figures 1d–1f then show the altitude h_{SC} , latitude λ , and longitude φ of MEX (positive eastward), respectively.

The oblique reflections seen in Figure 1a are labeled 1–4, and it is clear that these are observed over regions where the crustal field within the ionosphere is significant, $|\mathbf{B}|$ larger than ~ 50 nT, and is furthermore close

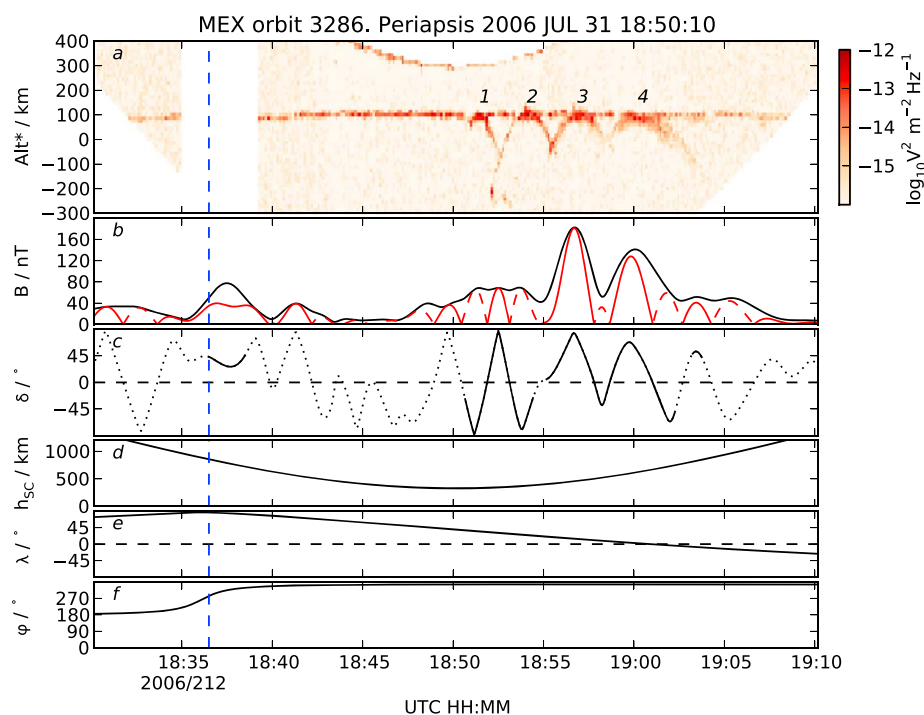


Figure 1. (a) MARSIS data from orbit 3286 on 31 July 2006, in which the reflected intensity at $f_s = 1.9$ MHz is color coded versus apparent altitude and time. Both the principal reflection from the nadir direction and several distinct oblique reflections are visible and annotated in the figure. Note a brief data gap from $\sim 18:35$ to $\sim 18:39$. The four oblique reflections detected on this orbit are labeled 1–4. (b) The *Lillis et al.* [2010] crustal magnetic field model, evaluated at fixed 150 km altitude below the position of the spacecraft. The black line indicates the total field strength $|\mathbf{B}|$, while the red line indicates the radial component B_r (shown dashed when B_r is of negative sign). (c) The inclination angle δ of the Martian crustal field with respect to the horizontal, shown dotted when the total field strength is less than 50 nT. (d–f) The altitude, planetographic latitude, and (East) longitude of MEX, respectively, along its orbit.

to vertical, $|\delta| \sim 90^\circ$. Each oblique reflection is observed for ~ 2 – 5 min duration, during which MEX travels ~ 500 – 800 km over the Martian surface. The first two such reflections appear to be associated with regions of fields for which $\delta \approx -90^\circ$ (field directed into the planet), while the last two are associated with fields of the opposite sense. The data gap present from 18:35 to 18:39 may have prevented the detection of an oblique echo corresponding to the region of intense yet nonradial crustal fields during the inbound segment of the orbit.

Duru et al. [2006] and *Gurnett et al.* [2005] showed that such oblique reflections were preferentially observed over regions for which Mars's crustal field inclination δ was expected to be almost vertical. Furthermore, they demonstrated that the difference in apparent altitude between the principal reflection and the apices of the hyperbolic oblique reflections was (almost) exclusively positive. Specifically, within the set of data examined, encompassing the interval 11 July 2005 to 27 January 2006, *Duru et al.* [2006] observed that the apices of $\sim 98\%$ of the observed oblique reflections were located at higher altitudes than the principal ionospheric reflection. *Gurnett et al.* [2005] and *Duru et al.* [2006] have suggested that such a distribution can only result if, for the overwhelming majority of cases, the trajectory of MEX is such that the spacecraft passes directly over the oblique reflection source and that these sources are themselves elevated over the background ionosphere. While there is no preferred horizontal symmetry axis for the regions of near-radial field produced in the Martian crust, MEX's elliptical polar consequently favors the detection of oblique reflections from regions that have a predominately zonal symmetry (i.e., are aligned East-West). A theoretical model embodying these two concepts was first presented by *Gurnett et al.* [2005] and is illustrated in Figure 2. An ionospheric "upwelling" is present in a region of near-vertical crustal fields, and the resulting distortion of otherwise horizontal plasma density gradients provides a source of oblique reflections. Within this picture, MEX is moving within the plane of the figure, and the ionospheric upwelling is present along the axis into and out of the plane. The structure of the upwelling is therefore determined by the structure of the crustal

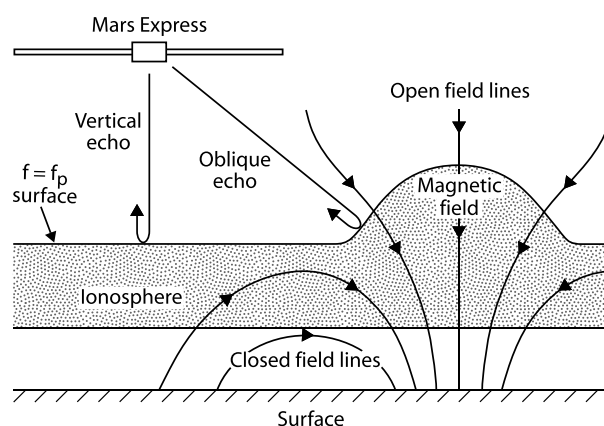


Figure 2. Illustration of an ionospheric structure that gives rise to an oblique reflection, as proposed by Gurnett *et al.* [2005] and Duru *et al.* [2006]. Surfaces of constant ionospheric plasma density bound the shaded region. Taken from Duru *et al.* [2006, Figure 3]. Copyright AGU, reproduced with permission.

fields, which while varied, has extended regions in which the field is both intense (>100 nT at 150 km altitude) and the field inclination angle δ is near vertical.

Considering the evolution of the apparent distance to the source of an oblique reflection observed sequentially during multiple MARSIS ionograms, Nielsen *et al.* [2007b] showed that the source location can be inferred due to the relatively rapid motion of the spacecraft, under the assumption that the source is itself stationary. The locus of possible sources of an oblique reflection detected in a single MARSIS ionogram, at a single frequency, is given by the intersection of a sphere centered on the spacecraft, and the corresponding isodensity surface in the ionosphere (through equation (1)). For oblique reflec-

tions present in sequential MARSIS ionograms, these loci will intersect at one or two points, indicating consistent source locations.

The process by which these large-scale ionospheric structures arise remains to be directly determined. It has been suggested that the precipitation of solar wind plasma (via the Martian magnetosheath) could lead to additional ionospheric heating, locally increasing the ionospheric scale height and thereby the density at fixed altitude [Ness *et al.*, 2000; Krymskii *et al.*, 2004]. Gurnett *et al.* [2005] subsequently suggested that these localized ionospheric upwellings may give rise to the oblique reflections detected in regions where the crustal field is such that precipitation of magnetosheath plasma into the ionosphere is feasible. Studies based primarily on MGS magnetometer data have yielded accurate maps of the extremely varied Martian crustal magnetic field [e.g., Acuña *et al.*, 1999; Purucker *et al.*, 2000; Arkani-Hamed, 2001; Cain *et al.*, 2003; Langlais *et al.*, 2004; Lillis *et al.*, 2008, 2010]. These spatially localized fields are, in places, sufficiently intense to dominate over the draped IMF and exert significant influence on ionospheric plasma properties and processes [e.g., Withers *et al.*, 2005; Fränz *et al.*, 2006; Nilsson *et al.*, 2006; Brain *et al.*, 2007]. On the dayside, stronger crustal fields allow more efficient vertical plasma transport [Andrews *et al.*, 2013], are associated with modulations in the position of the magnetic pile up boundary and bow shock [Crider *et al.*, 2002; Brain *et al.*, 2005; Edberg *et al.*, 2008, 2009], and may ultimately play some role in mediating the escape of atmospheric material [Fränz *et al.*, 2010; Nilsson *et al.*, 2011; Lundin *et al.*, 2011].

In this paper, we perform an initial survey of the repeatability of these oblique reflections, utilizing the regularity of the MEX orbit to systematically assess the location and size of the ionospheric structures that give rise to these radar signatures. We investigate the repeatability of the detection of oblique reflections originating from the same underlying ionospheric structure. Through this, we implicitly investigate the influence of external factors (chief among them, the state of the upstream solar wind and IMF) on the formation of these structures. We do not here investigate the influence of longer-term (i.e., seasonally or solar cycle controlled) variations in these ionospheric structures.

2. Extended Observations of Oblique Reflections

2.1. Overview

In wishing to examine the repeatability, or lack thereof, of the ionospheric structures that give rise to these oblique reflections, the frequency with which the same region of the ionosphere can be examined, under similar conditions and viewing geometry is of central importance. Typically on a single orbit, MARSIS will be switched between its two operating modes, with subsurface operations favored on those periapsis intervals at high-solar zenith angles (where the performance of the subsurface mode is markedly improved). When scheduled, AIS operations cumulatively account for $\sim 40\%$ of the total time the experiment is active, though on a single orbit this fraction can be up to 100%.

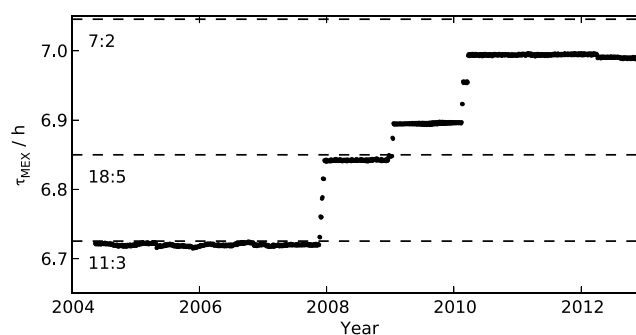


Figure 3. MEX orbital period τ_{MEX} plotted versus time, shown computed for every tenth orbit. Horizontal dashed lines indicate resonances with the rotation period of the planet.

the spacecraft trajectory information shown in Figures 1d–1f. From $\sim 18:36$ and continuing through periapsis at $\sim 18:50$, the spacecraft traverses $\sim 110^\circ$ of latitude from the northern pole down through the equator, while the longitude of the spacecraft remains at an approximately constant $\sim 340^\circ$. Thus, in order to study the sources of the frequently detected oblique reflections with their apparent longitudinal structure, the inclined nature of the MEX orbit can be exploited to allow a portion of the MARSIS AIS data to be interpolated and plotted versus apparent altitude and latitude (rather than UTC), at approximately constant longitude. For the example orbit shown in Figure 1, the portion of the AIS data taken on this periapsis pass that can be transformed in this manner is that to the right of the vertical dashed blue line, for which the spacecraft latitude is monotonically decreasing with time.

The orbital period of MEX τ_{MEX} dictates the number of orbits that will elapse between repeated passes over the same region of longitude. This quantity is not fixed but has increased in steps since the beginning of the orbital tour, as shown in Figure 3. During the first few years of operations at Mars, MEX's altitudes of periapsis and apoapsis were ~ 300 and $\sim 10,100$ km, respectively, and the corresponding orbital period of the spacecraft was ~ 6.7 h. Subsequently, the altitude of the orbit has increased, with periapsis now at altitudes of ~ 360 km and apoapsis of 10,500 km, and the orbital period has consequently increased to its current value of ~ 7.0 h. Horizontal dashed lines in Figure 3 indicate the three lowest order resonances $N_{\text{MEX}} \cdot N_{\text{Mars}}$ between the spacecraft and the planet, being 11:3, 18:5, and 7:2. From 2004 to 2008 the spacecraft is closest to the 11:3 resonance ($\tau_{\text{MEX}} \approx 6.72$ h), such that every eleventh orbit revisits the same longitude meridian at periapsis after three Martian days (~ 74 h), to within $\sim 1^\circ$. An increase of the periapsis altitude at the end of 2007 leads to a corresponding lengthening of τ_{MEX} to ~ 6.84 h and establishment of an 18:5 resonance, maintained until early 2009. This affords repeated sampling of longitudes to within $\sim 2^\circ$ every eighteenth orbit. A subsequent, second raising of the periapsis altitude and further increase in τ_{MEX} to ~ 6.89 h breaks this resonance and yields an interval when no suitable low-order resonance is applicable, before a third change brings the spacecraft somewhat closer to the 7:2 resonance. However, during this period the separation in longitude between the periapses of every seventh orbit is $\sim 6^\circ$, substantially larger than that for the other resonances identified earlier in the mission.

With this information, at each point in the MEX mission we can identify an appropriate resonance with the rotation of the planet that can be used to organize the available AIS data into sequences of orbits. The sequence will comprise every 7, 11, or 18 orbits as appropriate, in which the data taken will yield coverage over a wide span of latitude, while the longitude of the observations will remain approximately constant, drifting only slowly from one orbit in the sequence to the next. At the same time, owing to the relatively slow motion of the MEX orbital plane compared to these resonances, the local time and solar zenith angle coverage will also only change slowly during the orbits in the sequence. Conversely, over the several days that will elapse between each orbit in the sequence the conditions of the interplanetary medium upstream, though poorly resolved by the appropriate instruments on MEX (e.g., due to the lack of a vector magnetometer), cannot be reasonably expected to remain static.

The restricted operation of MARSIS in AIS mode necessarily imposes limits to the lengths of such “runs” of ionospheric soundings over particular regions of the surface that can be achieved. The useful operating window of the radar on a given orbit is dictated by the spacecraft altitude, as the maximum range within

In addition to the restrictions imposed by the operating modes of the instrument, the MEX orbital configuration has significant influence on the degree to which the same ionospheric region can be repeatedly sounded. MEX orbits Mars in an elliptical polar orbit, inclined to the planet's equatorial plane by $\sim 86^\circ$. As a consequence of this highly inclined orbit, during much of the periapsis segment of its orbit, MEX rapidly traverses a large span of latitude while remaining at near-constant longitude. This can be seen directly from

which an ionospheric structure can be detected is ~ 1100 km. For the nominal orbit of MEX, this translates to a period of ~ 20 min either side of periapsis, or approximately ~ 320 individual AIS soundings. Hereafter, we define orbits on which at least 200 distinct AIS soundings were obtained as being “complete” and do not consider those orbits with fewer than this number. Furthermore, we consider only those soundings performed over the dayside ionosphere away from the terminator (solar zenith angle (SZA) $< 90^\circ$), such that the background ionosphere is at least reasonably well established. To obtain sequences of complete orbits of a meaningful length (at least five), we allow for a maximum of two incomplete orbits consecutively at any point within the sequence. If more than three orbits elapse when no AIS data are taken at the required location in the sequence, we consider the sequence broken and the intervening evolution of the MEX orbit (in SZA and subspacecraft longitude) too large to allow meaningful comparisons to be made across the sequence. So defined, of the ~ 1480 complete AIS orbits available, 634 of them were organized into 81 separate sequences, each containing a median of seven orbits. Sequences of less than five orbits were not considered, and these comprise the majority of the remaining ~ 850 orbits that were not further analyzed. Of these 634 orbits, oblique reflections were clearly detected on all but 192, and only 7 of the 81 sequences showed no oblique reflections on any of their constituent orbits. Each of these 81 separate sequences having been examined in detail, in the following sections we present three examples which illustrate interesting properties of the oblique reflections not yet reported, including their striking stability.

2.2. Sequence 1

In Figure 4 we show an example of one such sequence of 10 MEX orbits during which at least 200 AIS soundings were performed, each centered around the $\sim 210^\circ$ meridian. These data were taken during the period 12 February to 3 April 2008, during which the MEX orbit period was close to the 18:5 resonance with the rotation of the planet. Every eighteenth orbit is plotted, numbered from 5283 to 5463, and the observations thus span a period of ~ 51 days (~ 50 Mars rotations), with the start and end of the sequence being dictated by the lack of availability of AIS data on the required orbits. We allow for the absence of one orbit of AIS data within the sequence, as only an incomplete complement of AIS data were obtained on orbit 5445. In Figures 4a–4j we show the reflected signal received by the radar at 1.9 MHz color coded versus both apparent altitude and latitude of the observation, for each of these orbits. Data are only shown for the part of the periapsis segment of each orbit where the latitude is monotonically decreasing with time, and the longitude is approximately constant. The data are then interpolated and plotted versus latitude, with this interpolation being very close to linear. In Figure 4k we combine measurements made on the individual orbits in the above panels, showing the number of orbits N for which the reflected intensity is greater than $10^{-15} \text{ V}^2 \text{ m}^{-2} \text{ Hz}^{-1}$ at each sampled point in apparent altitude and latitude. Finally, Figures 4l and 4m show the longitude and solar zenith angle of each orbit, respectively, with the red and blue traces in each panel corresponding to the first and last orbits within the sequence, respectively. It can be seen from Figures 4l that, within this sequence of 10 orbits, the longitude of the spacecraft drifts westward (to earlier longitudes) from one to the next by $\sim 3^\circ$. Simultaneously, the SZA sampled at each latitude steadily decreases, with the most substantial drift occurring at $\sim 20^\circ$ latitude. This presentation format is retained for subsequent related figures.

Beginning with the data from orbit 5283 shown in Figure 4a, we first note that the horizontal principal reflection from the stratified subspacecraft ionosphere is well resolved throughout the periapsis pass. Second, at least two clear oblique reflections are present, with their apices at latitudes of approximately -19° and -6° , with the latter being more clearly identifiable from its well-defined quasi-hyperbolic trace. This second oblique reflection is clearly seen to extend over ~ 200 km in apparent altitude and $\sim 15^\circ$ in latitude. A strikingly similar oblique echo feature is subsequently detected 18 orbits later (Figure 4b), centered again at a latitude of -6° on orbit 5301, and reappears clearly for the next four orbits in the sequence (Figures 4c–4f), only disappearing when the increasing latitude of periapsis removes this latitude band from the radar’s field of view on orbit 5409. Though somewhat less clear, the oblique reflection observed at a latitude of -19° on 5283 is perhaps repeatedly encountered on the two orbits that follow. Further reflections that cannot be attributed to a horizontally stratified ionosphere are detected later in the sequence and at northern latitudes, e.g., on orbit 5373, without a clear relationship to the oblique reflections (or lack thereof) detected on the preceding and following orbits.

Turning to the summed data shown in Figure 4k, aside from the horizontal principal reflection, the only other significant feature is the oblique reflection centered at -6° latitude. Little spread in the position of this oblique reflection is observed, strongly suggesting that the latitude of the ionospheric feature that gives rise

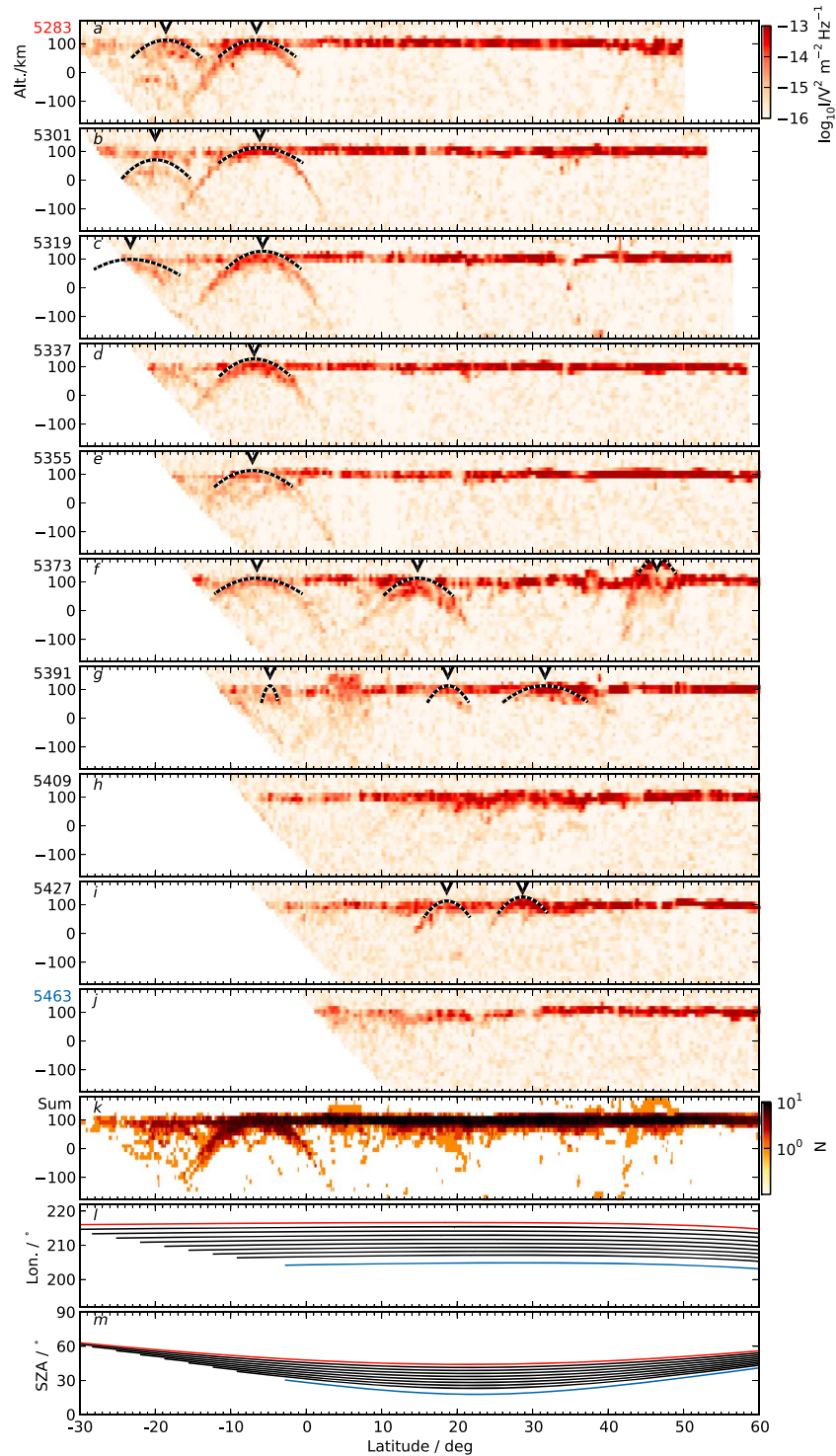


Figure 4. MARSIS AIS data taken on orbits 5283–5463. (a–j) The received intensity of the ionospheric reflections at 1.9 MHz is shown color coded versus apparent altitude and interpolated latitude. Where determined, quadratic fits to the observed oblique reflections are shown by the black lines and white dotted lines. Inverted triangular icons at the upper edge of each panel indicate the locations of the apices of each fitted oblique reflection. (k) Color coded the number of orbits N for which the reflected intensity at a given apparent altitude and latitude is above $10^{-15} \text{ V}^2 \text{ m}^{-2} \text{ Hz}^{-1}$. (l and m) The longitude and SZA of the spacecraft on each orbit, with the red and blue lines in each panel corresponding to the first and last orbits in the sequence, respectively.

to this reflection does not substantially change over the ~ 6 orbits (~ 30 days) for which it is observed. We can also conclude that, as the evolution of the longitude of MEX during this period is small yet significant, spanning some $\sim 15^\circ$, the underlying ionospheric structure has a large degree of symmetry in the zonal (East-West) direction.

In order to characterize the oblique reflections, we approximate their hyperbolic reflection trace by a quadratic polynomial (for simplicity and to provide commonality with previous work by *Duru et al.* [2006]). The fit can therefore be expressed as

$$h(t) = \tau(t - t_0)^2 + h_0, \quad (2)$$

where h_0 and t_0 delimit the apex position in apparent altitude h and time t , respectively, and τ can be interpreted as a “shape parameter.” The three independent parameters in equation (2) are determined for each observed oblique reflection by first manually approximating h_0 and t_0 . In the vicinity of the manually selected apex position, h_0 , t_0 , and τ are each varied within reasonable limits, until the integrated reflection intensity between $h(t)$ and $h(t) - \Delta h$ is maximized. In principal, any value of Δh greater than 14 km can be used, this being the vertical resolution available. Experimentation has shown that a somewhat larger value yields more accurate and stable fits, since the oblique reflection traces typically extend over a broad range of apparent altitude (likely reflecting the presence of small-scale irregularities embedded in the larger ionospheric structure that is producing them). We therefore take Δh to be ~ 70 km, or five apparent altitude bins, representing a reasonable upper limit to the “thickness” of the oblique reflection trace in apparent altitude.

Where determined, fits to the oblique reflections are shown overplotted on the data by the black and white dotted lines in Figures 4a–4j. These fits are shown symmetric about the apex of the oblique reflection, such that any departure from symmetry can be clearly resolved through comparison of the fit with the data. Triangular icons are shown along the upper edge of each panel indicating the location in latitude of the apex of each oblique reflection. It can be seen that while the larger oblique reflections, having traces which extend over ~ 10 or more degrees of latitude are generally well fitted, the shapes of those smaller, more transient features are often only poorly approximated by this technique. Clearly, each oblique reflection trace must be present over a reasonable extent of spacecraft latitude and clearly distinguishable from the principal ionospheric reflection for part of this time in order for a reasonable fit to be obtained. To ensure this, we only further consider those oblique reflections whose trace is clearly separate from the principal reflection for at least ~ 5 successive AIS soundings. We note that we do not necessarily require the oblique reflections to be symmetric about their apices.

The fits obtained are used primarily as a mechanism to track the location in space and time of the apex of each observed oblique reflection. The value of the shape parameter τ is determined both by the horizontal geometry of the underlying ionospheric structure and the relative motion of the spacecraft. Furthermore, it is the least reliably fitted parameter by this method, particularly for those oblique reflections which are either only briefly or partially observed. Consequently, we leave a fuller analysis of the horizontal and vertical structures of the sources of oblique reflections for a future paper.

In Figure 5 we show maps of the inclination angle of the Martian crustal magnetic field, alongside the mapped position of the observed oblique reflections observed in Figure 4. Figure 5a shows the magnetic field inclination angle δ evaluated from the *Lillis et al.* [2010] field model at fixed 400 km altitude, color coded such that shades of grey and red indicate regions of negative (inward) and positive (outward) fields, respectively. Regions within which $\delta \approx 0^\circ$ indicate near-horizontal fields. The 400 km altitude was selected as it corresponds to the altitude of the MGS spacecraft during the mapping phase of its mission, during which the magnetometer data used in construction of the *Lillis et al.* [2010] field model were obtained. The solid, dashed, and dotted contours bound regions in which the total magnetic field strength $|\mathbf{B}|$ is greater than 20, 50, and 100 nT, respectively, as indicated on the upper edge of the figure. Three regions of the map are separately replotted in the lower panels of Figure 5, showing both the trajectory of MEX and the observations of oblique reflections within this and following sequences examined in this paper. Ground tracks of the 10 orbits shown in Figure 4 are shown in Figure 5b, color coded according to the apparent altitude of the observed oblique reflections (darker blues thus indicating close approaches to an oblique reflection site). For presentation purposes we have used a faded color scheme to represent the underplotted crustal field inclination angle within these subplots.

For those most distinct oblique reflections noted previously at latitudes of $\sim -6^\circ$ in Figure 4, it can be seen that the structure detected on sequential orbits falls on an approximately East-West aligned axis, as

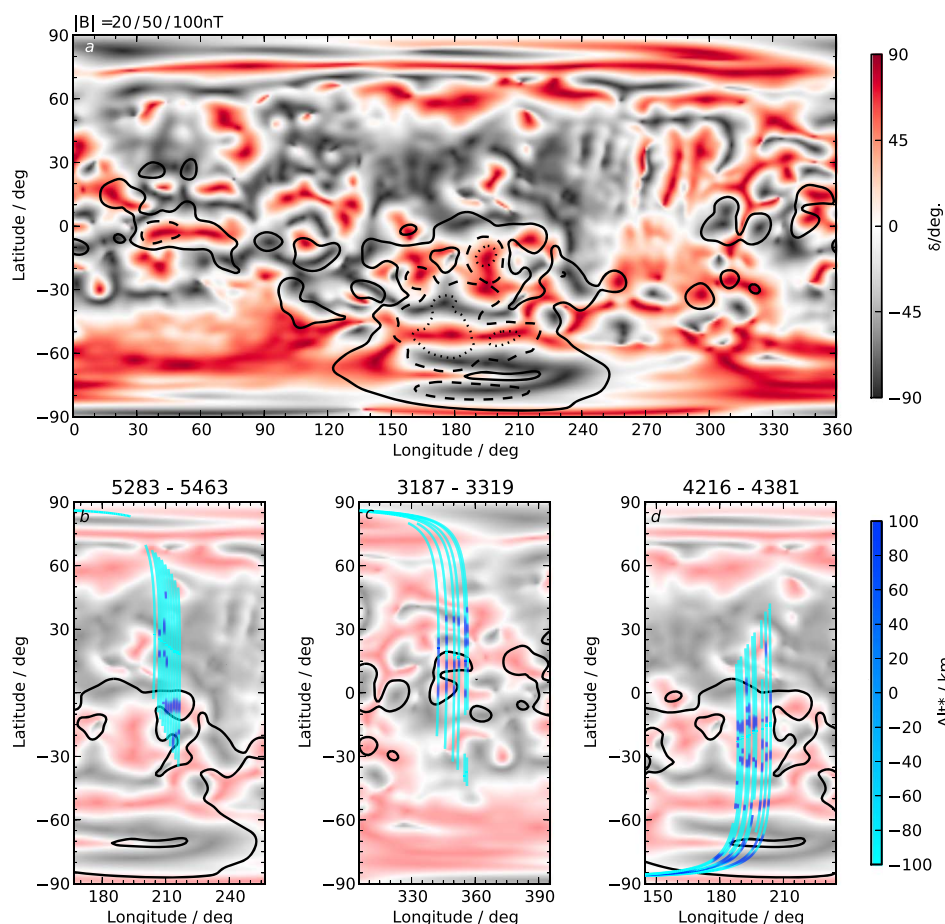


Figure 5. (a) Map of the magnetic field inclination angle δ determined from the *Lillis et al.* [2010] crustal field model, computed at 400 km altitude. Overplotted solid, dashed, and dotted lines show contours of the corresponding total field strength $|\mathbf{B}|$ at values of 20, 50, and 100 nT, respectively. (b–d) Replotted subregions of the larger map, though only the $|\mathbf{B}| = 20$ nT contour is retained, and the color code used for the underplotted magnetic field inclination angle is muted for ease of presentation. The ground track of MEX is shown in Figure 5b for each of the 10 orbits from which AIS data were shown previously in Figure 4. These tracks are color coded according to the apparent altitude of any oblique reflections detected, such that oblique reflection sources appear red or yellow. Intervals for which AIS data were not taken during a given orbit can be seen as gaps within these color-coded lines. Figures 5c and 5d follow the same format as Figure 5b but instead show ground tracks and oblique reflections detected on orbits shown later in Figures 6 and 7.

expected from the results of *Duru et al.* [2006]. The crustal magnetic field along the axis of this structure is near vertical (of positive radial sense), having strengths of ~ 20 – 50 nT (cf. Figure 5a). The evolution of the MEX orbit, and the gradual progression of periapsis to higher northern latitudes during this set of observations, likely precludes the detection of this same oblique echo during the latter orbits in the sequence. Additionally, closer inspection of the local configuration of the magnetic field inclination also suggests that this area of positive inclinations ceases at its western edge, and the ionospheric structure may well terminate part way through this sequence owing to the slow westward drift of periapsis (i.e., to earlier longitudes) during the sequence. Additional oblique reflections less clearly resolved at higher latitudes in Figure 4 may be associated with the smaller, confined regions of outward directed vertical fields crossed later in each orbit. We do not see any evidence for repeated detections of ionospheric structures originating from northern latitudes, within the range of longitudes sampled in this sequence. The generally weaker crustal fields encountered in the northern hemisphere could conceivably have lead to the intermittency of detection of these oblique reflections.

2.3. Sequence 2

In Figure 6 we show a second sequence of MARSIS AIS data obtained on six orbits. These data were taken between 3 July and 9 August 2006 (orbits 3187 to 3319) during a ~ 37 day interval. Each sequential orbit

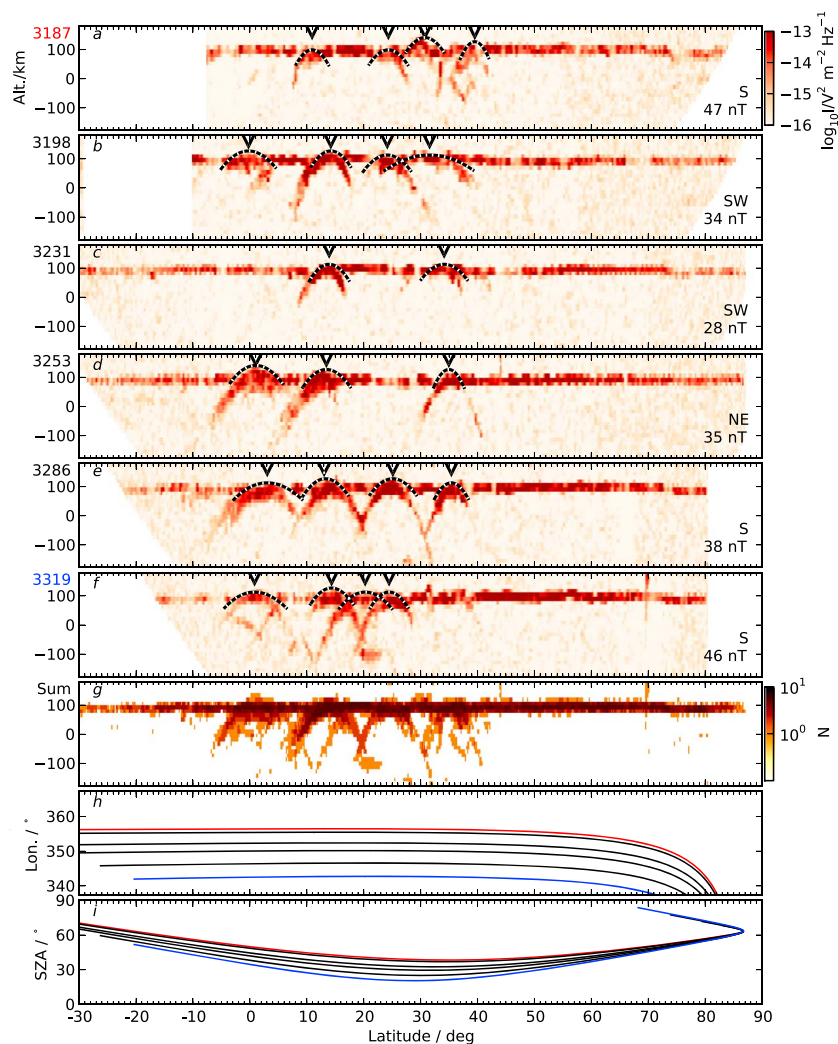


Figure 6. (a–i) MARSIS AIS data taken on orbits 3187–3319, presented in the same format as used in Figure 4.

shown in Figure 6 is spaced by an integer multiple of 11 orbits from the preceding, and we note that within this sequence a substantial fraction of the otherwise interleaving orbits are not shown, as no AIS soundings were performed (i.e., only every 22nd or 33rd orbit is shown). Nevertheless, the shift in longitude between each orbit in the sequence as shown remains small, $< 3^\circ$. These orbits all have periapses in the northern hemisphere, at longitudes of $\sim 340^\circ$ – 360° . Referring back to the map of the crustal field strength and orientation shown in Figure 5a, this region can be seen to be comprised of generally weaker crustal magnetic fields than in the opposing (southern) hemisphere, though the typical field strengths are not negligible in comparison to the typical draped IMF at these altitudes. Furthermore, this particular sequence is one of only a few obtained when MGS was simultaneously operating at Mars, affording a better estimate of the IMF conditions upstream (MGS operations ceased in late 2006).

We note that the data from orbit 3286, shown in Figure 6e, are essentially identical to those shown previously in Figure 1a. However, in Figure 6 the data are shown reversed, such that the latitude of the observation now increases from left to right along the page (as was similarly the case in Figure 4). Additionally, the brief segment of AIS data that was shown at the leftmost edge (earliest time) in Figure 1 is not displayed in Figure 6, as (for this sequence) only those data obtained while the spacecraft latitude was monotonically decreasing with time were considered. The format used in Figure 6 is otherwise identical to that used previously in Figure 4.

Multiple quasi-hyperbolic oblique reflections are clearly present on each orbit within this sequence, and the principal reflection from the horizontally stratified ionosphere is again generally well resolved. The clearest

and most persistent oblique reflection appears to be that with its apex at $\sim 13^\circ$ northern latitude. Consequently, this feature is also strongly visible in the summed data shown in Figure 6g, along with at least three other similar hyperbolic traces centered on latitudes of $\sim 0^\circ$, $\sim 24^\circ$, and $\sim 36^\circ$. Within the individual orbits shown, these three other features are each visible on four or five of the six possible orbits, indicating that the sources giving rise to these reflections have significant longitudinal extents.

As was noted, data from the magnetometer and electron reflectometer instrument package on MGS are available throughout this interval, from which the IMF orientation and draped magnetic field strength can be inferred, through the use of proxy measurements made within the Martian system [Crider *et al.*, 2003; Brain *et al.*, 2005, 2006]. Proxies are required in this process simply because, during this phase of the MGS mission, the spacecraft was orbiting at an approximately constant altitude of ~ 400 km, and hence rarely entered the solar wind. Full details of the derivation of the upstream IMF orientation (the so-called “clock angle”) and the magnetic field strength at the subsolar point are provided by Brain *et al.* [2005, 2006]. For each orbit of AIS data shown in Figure 6, the nearest determined MGS proxies are indicated in the lower right of each panel, where we have expressed the orientation by the nearest compass point (representing the relatively large uncertainty in this parameter). We note that the cadence with which the MGS proxies are determined is that of the MGS orbital period, ~ 2 h, such that each data point represents an average of the upstream conditions over a period significantly longer than that within which the AIS soundings are performed. Significant variability in the upstream pressure and magnetic field is generally to be expected yet is not reflected in these proxies.

For all orbits in the sequence presented in Figure 6, the corresponding MGS data suggest that the IMF is oriented southward to south-westward with respect to Mars, with the draped magnetic field at the subsolar point having an intensity of ~ 35 – 45 nT. The only significant exception occurs during orbit 3253 (Figure 6d), in which the IMF orientation is seen to be approximately oppositely directed as compared to the rest of the sequence. During this orbit, three oblique reflections are still clearly detected, which all bear clear relationships to those observed in both earlier and later orbits in the sequence. Furthermore, we cannot discern any substantial shifts in the latitudinal location of the apices of the oblique reflections observed on this orbit, as compared to those seen elsewhere in the sequence.

As previously, we perform manually guided fits to each clear oblique reflection, with the resultant fitted traces indicated by the black and white dashed lines in the upper panels of Figure 6. Ground tracks indicating the apparent altitude of the fitted oblique reflections are then shown for each of the six orbits in the sequence in Figure 5c. A clear correspondence is again seen between the features observed and the regions of relatively intense and nearly vertical crustal magnetic fields, despite the generally weaker field strengths present in this region. Those oblique reflections seen at higher northern latitudes within this sequence are somewhat more varied, possibly reflecting the generally weaker crustal fields in this area. Conversely, an oblique reflection is detected on the part of each orbit that passes within the contoured region of near-vertical crustal fields $|\mathbf{B}| > 20$ nT. Furthermore, it can be reasonably argued that even the subtle shifts between observations of oblique reflections of 1° – 2° of latitude between adjacent orbits are reflective of the underlying structure in the crustal fields.

2.4. Sequence 3

The final sequence of AIS observations shown in this paper were taken throughout 10 orbits (4216 to 4381), obtained during an interval of ~ 46 days between 18 April and 3 June 2007. The data are shown in Figure 7, in the same format used previously in Figures 4 and 6. This sequence possesses the most complete coverage of the region of strongest crustal magnetic fields centered near $\sim 180^\circ$ longitude in the southern hemisphere available within the wider AIS data set. In comparison to those sequences shown previously in this paper, it is readily apparent from the data shown that the oblique reflections are detected both more frequently in this region and furthermore that they are more varied in their appearance. At least four distinct oblique reflections can be seen on each orbit. Unfortunately, the abundance of oblique reflections and the frequent significant overlaps in their reflection traces that result makes analysis of their characteristics somewhat more subjective than those shown previously. Nevertheless, repeatedly detected quasi-hyperbolic structures are clearly present in the summed reflection data shown in Figure 7k, and we note specifically those persistent features seen at latitudes of $\sim -77^\circ$, $\sim -53^\circ$, and $\sim -14^\circ$.

The mapped apparent altitudes of these fitted oblique reflections are shown in Figure 5d. Once again, a clear association is seen between the observed locations of the oblique reflections and regions of intense

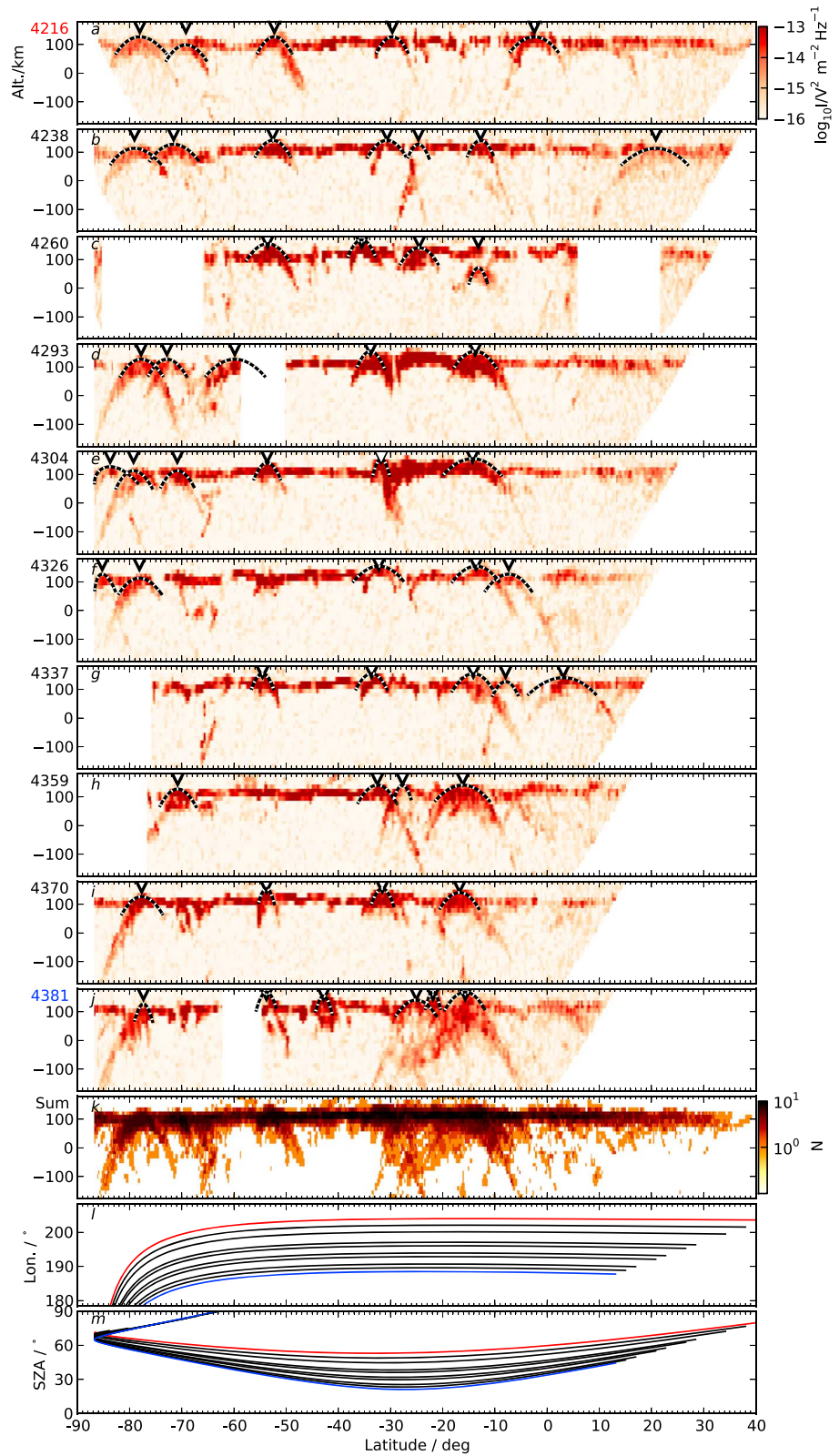


Figure 7. (a–m) MARSIS AIS data taken on orbits 4216–4381, presented in the same format as used in Figure 4.

near-vertical crustal magnetic fields (irrespective of the sign of the vertical component). The combination of the map projection used and the high southern latitudes reached by the spacecraft within this sequence of orbits lead to an exaggeration of the length scale over which the oblique reflections are observed. Nevertheless, the oblique reflection source centered at latitudes close to $\sim -80^\circ$, clearly detected on every orbit within the sequence for which AIS soundings were performed, is justifiably associated with an extended region of intense ($|\mathbf{B}| > 50$ nT) radial field. However, those intermittently detected oblique reflections seen at lower latitudes, close to $\sim -70^\circ$, show much less of a correspondence to vertical fields. These oblique reflections arise from a region of relatively weaker crustal fields, where the field orientation is much closer to horizontal. Similarly, it is interesting to note that the longitudinally extended region of near-radial fields at $\sim -64^\circ$ latitude does not appear to regularly produce oblique reflections, with only a single detection throughout the sequence. The same can be said about the similar region of near-radial fields that MEX traverses on these orbits at $\sim -42^\circ$ latitude. The apparent lack of oblique reflections at these locations may reflect variations in the magnetic field structure below the 400 km reference surface, indicating that the cusp-like fields observed at spacecraft altitudes do not persist down to ionospheric altitudes. Alternatively, this apparent discrepancy may be due to inaccuracies in the models of the Martian fields at ionospheric altitudes, owing to the incomplete coverage of the surface obtained with MGS below its mapping altitude of ~ 400 km. Recurrent oblique reflections are observed at high southern latitudes, and we note in particular the feature present at $\sim -77^\circ$ that can be clearly seen throughout the sequence of data shown in Figure 7. This suggests that the apparent lack of oblique reflections from the region of radial fields at higher latitudes is not some effect associated simply with high southern latitudes (or proximity to the pole). Elsewhere within the sequence, the correspondence between the crustal field orientation and the sites giving rise to oblique reflections is significantly clearer.

3. Summary

In addition to the reflection from the horizontally stratified Martian ionosphere below the spacecraft, the MARSIS radar onboard MEX regularly detects additional reflections at oblique incidence. These phenomena, first elucidated by *Gurnett et al.* [2005] and subsequently studied in detail by *Duru et al.* [2006], are produced when the transmitted sounding pulse is specularly reflected from a region of the ionosphere in which the surfaces of constant plasma density are tilted away from the horizontal. In this paper, we have carefully examined taken in sequences of multiple successive orbits which sampled the same regions of the Martian ionosphere, with only small, steady changes in the latitude, longitude, and solar zenith angle occurring between observations. In total, 634 orbits of MARSIS AIS data were examined, forming 81 separate sequences of multiple orbits covering similar regions of the dayside ionosphere. Of the 81 sequences examined, only seven showed no apparent oblique reflections on any of their constituent orbits. An average of ~ 2 oblique reflections per orbit were detected on the others. We presented three examples from these data, highlighting the observed behavior in representative regions of the Martian crustal field, including the most intense sources in the sources in the southern hemisphere, and those regions in the northern hemisphere where the field is largely insignificant.

In this section we briefly summarize the central results of this study.

1. Oblique reflections detected by the MARSIS radar can be reliably attributed to regions of near-radial crustal fields, which (at the altitudes of the spacecraft) are of sufficient strength to offset that of the draped IMF. The sources of these oblique reflections are likely regions in which the ionospheric plasma density is locally modified by some process as yet to be fully elucidated.
2. Through analysis of MARSIS AIS data obtained on multiple passes by MEX over the same regions of the Martian surface (which occurs with a cadence not less than several Martian days), we have investigated the repeatability of the underlying ionospheric structures that give rise to oblique reflections. Individual observations of oblique reflections, detected on multiple orbits, can often be reliably attributed to a single cusp-like region of the ionosphere. We conclude that the density structures responsible for the oblique echoes are therefore repeatedly formed in the dayside ionosphere during each planetary rotation, with broadly similar properties (e.g., spatial extent and peak density).
3. During a limited period of the MEX mission, it is possible to infer with reasonable accuracy the average state of IMF at Mars, using proxy data from MGS. During the example shown in this paper for which this was possible, while the IMF is expected to be broadly comparable between most observations, we note the presence of a single MEX orbit for which MGS reports a markedly different orientation of the IMF.

However, this appears to exert no significant influence on the observed oblique reflections. Moreover, throughout all the observations presented in this paper, we can expect that similar variations are routinely present in both the orientation and strength of the IMF, and the bulk parameters of the solar wind, on a range of timescales much shorter than the few days that typically elapse between MEX's repeated visits to the same region of the Martian ionosphere. The apparent stability of the sources of these oblique reflections therefore suggests that the degree to which they are controlled by the conditions upstream of the Martian-induced magnetosphere is small.

4. Repeated oblique reflections are additionally detected from regions in the northern hemisphere of Mars, where the crustal field at ionospheric altitude is generally much weaker, and would therefore be more readily influenced by the instantaneous orientation and strength of the IMF.

4. Discussion

The results of this study serve to further expose the properties of the Martian ionosphere, and its interaction with the planet's highly varied crustal magnetic field. In this section, we briefly comment upon a few of these results and discuss their wider implications.

First, the central result of this study is that the plasma density structures that give rise to oblique echoes are themselves stable, repeatable features embedded in the dayside ionosphere. Each sequence of observations presented typically lasted several tens of days such that, while the relevant orbital parameters changed only slightly, it is likely that the configuration of the Martian-induced magnetosphere can have evolved substantially within each sequence in response to the highly variable solar wind and IMF conditions on these timescales [see, e.g., *Dubinin et al.*, 2008, 2009; *Edberg et al.*, 2009; *Opgenoorth et al.*, 2013]. The potential impact of large rotations, changes in intensity, or discontinuities in the IMF upon the process producing these ionospheric structures therefore seems small and certainly insufficient to completely control their formation (or conversely, their inability to form). While intermittent or isolated oblique reflections are sometimes detected in regions of weaker crustal fields, in particular, in the northern hemisphere of Mars, it remains the case that stable oblique reflections are sometimes detected in regions where the crustal field has a cusp-like configuration but is not of sufficient strength to reliably dominate that of the draped IMF. Furthermore, the apparent stability of the underlying ionospheric density structures provides an important constraint upon theories of their origin.

Overall, the appearance of a given oblique reflection can generally be understood as being principally controlled by the underlying structure of the crustal magnetic field in the ionosphere. While the structures examined in this study generally exhibit an extent along the East-West (zonal) direction, small yet well defined tilts away from this axis are sometimes present over regions where the crustal field inclination displays similar tilts. The configuration of the MEX orbit and the requirement for isosurfaces of ionospheric plasma density perpendicular to the radar sounding pulse imposes some limits on the shape of ionospheric structures from which oblique reflections can be detected, which future studies will need to address, likely through the use of ray-tracing codes.

Following *Ness et al.* [2000] and *Krymskii et al.* [2004], *Gurnett et al.* [2005] have suggested that the required ionospheric elevations or upwellings could be the result of a combination of ionospheric heating and impact ionization due to precipitation of magnetosheath plasma. Whether this process can supply a sufficiently continuous production of ionospheric plasma above that of photo-ionization or supply sufficient energy to produce the observed vertical displacements of the ionospheric plasma remains to be fully investigated. In considering the role that precipitation and subsequent impact ionization may play in establishing the ionospheric structures which produce these oblique reflections, we note that a qualitatively similar dependence on magnetic field orientation has been found by *Němec et al.* [2010, 2011] in studies of localized patches of ionization observed in the Martian nightside ionosphere. Typical plasma densities within these areas of radial crustal fields in the deep nightside ($\text{SZA} < 125^\circ$) are at most $\sim 10^4 \text{ cm}^{-3}$, somewhat lower than the $4 \times 10^4 \text{ cm}^{-3}$ density surface in which the structures presented in this paper are embedded within. Moreover, we note that the structures studied in this paper frequently have corresponding signatures at significantly higher densities (frequencies above the 1.9 MHz selected here), indicating continuation of these irregularities down toward the altitude of the main ionospheric peak. Similarly, modeling studies have thus far shown that while particle precipitation into the nightside ionosphere and subsequent electron impact ionization may be sufficient to produce the observed plasma densities past the terminator,

reasonable estimates also suggest that significant modifications of the dayside ionosphere are not possible through this mechanism alone [Fillingim *et al.*, 2007; Lillis *et al.*, 2009, 2012; Lillis and Brain, 2013]. If electron precipitation is of central importance in establishing these ionospheric structures on the dayside, it must be via some indirect route, for example, via increases in ionospheric electron temperature and corresponding reductions in the ion-electron recombination rate [Nielsen *et al.*, 2007a]. More detailed estimates of the role of electron precipitation will be possible with more developed measurements of ionospheric electron temperature.

In this context we note that ionospheric upwellings observed by both ground and space-based radar techniques at Earth are often attributable to Joule-heating processes, arising as a result of electrical currents and corresponding perpendicular electric fields E_{\perp} at ionospheric altitudes. Specifically, the Joule-heating rate Q at altitude h is given by

$$Q(h) = \mathbf{J} \cdot \mathbf{E} = \mathbf{J}_{\perp} \cdot \mathbf{E}_{\perp} = \sigma_p(h) E_{\perp}^2(h), \quad (3)$$

where σ_p is the ionospheric Pedersen conductance. (Hall currents do not contribute to the heating rate, and we assume no parallel electric fields are present within the ionosphere itself. The potential impacts of Joule heating driven by field-aligned currents upon the ionosphere and neutral atmosphere have most recently been demonstrated in data taken with the CHAMP spacecraft at Earth [see, e.g., Lühr *et al.*, 2004; Liu *et al.*, 2005].) Through analysis of MGS magnetometer data, Opgenoorth *et al.* [2010] produced altitude profiles $\sigma_p(h)$ for various configurations of the Martian crustal magnetic field, showing that in regions where the crustal field is weak, two peaks in $\sigma_p(h)$ are present at altitudes of ~ 125 and 190 km (i.e., both at and well above the ionospheric peak density, respectively). Elsewhere, in regions of strong crustal fields, the lower altitude peak in $\sigma_p(h)$ is not present, implying that Joule heating is relatively more efficient at higher altitudes above the main ionospheric peak. Qualitatively, this agrees with our observation that the ionospheric plasma structures that give rise to oblique reflections are more generally located well above the ionospheric peak.

The full details of the ionospheric plasma structures that produce these oblique reflections will likely be much more apparent following in situ samples of the Martian ionosphere that will be made by the upcoming NASA MAVEN spacecraft. In particular, joint analysis of data from both the MARSIS radar on MEX and complementary in situ measurements made by the MAVEN instrument suite will hopefully provide significant further understanding of the physical processes responsible for this phenomenon.

Acknowledgments

D.J.A., H.J.O., M.A., and N.J.T.E. acknowledge funding from the Swedish National Space Board. The research at the University of Iowa was supported by NASA through contract 1224107 from the Jet Propulsion Laboratory. Data used in this study are available on the ESA Planetary Science Archive.

Masaki Fujimoto thanks Paul Withers and Robert Lillis for their assistance in evaluating this paper.

References

- Acuña, M., *et al.* (1999), Global distribution of crustal magnetization discovered by the Mars Global Surveyor MAG/ER experiment, *Science*, 284(5415), 790–793.
- Andrews, D. J., H. J. Opgenoorth, N. J. T. Edberg, M. André, M. Fränz, E. Dubinin, F. Duru, D. Morgan, and O. Witasse (2013), Determination of local plasma densities with the MARSIS radar: Asymmetries in the high-altitude Martian ionosphere, *J. Geophys. Res. Space Physics*, 118, 6188–6196, doi:10.1002/jgra.50593.
- Arkani-Hamed, J. (2001), A 50-degree spherical harmonic model of the magnetic field of Mars, *J. Geophys. Res.*, 106, 23,197–23,208, doi:10.1029/2000JE001365.
- Brain, D. A., J. S. Halekas, R. Lillis, D. L. Mitchell, R. P. Lin, and D. H. Crider (2005), Variability of the altitude of the Martian sheath, *Geophys. Res. Lett.*, 32, L18203, doi:10.1029/2005GL023126.
- Brain, D. A., D. L. Mitchell, and J. S. Halekas (2006), The magnetic field draping direction at Mars from April 1999 through August 2004, *Icarus*, 182, 464–473, doi:10.1016/j.icarus.2005.09.023.
- Brain, D. A., R. J. Lillis, D. L. Mitchell, J. S. Halekas, and R. P. Lin (2007), Electron pitch angle distributions as indicators of magnetic field topology near Mars, *J. Geophys. Res.*, 112, A09201, doi:10.1029/2007JA012435.
- Budden, K. G. (1961), *Radio Waves in the Ionosphere*, 2009 ed., Cambridge Univ. Press, Cambridge, U. K.
- Cain, J. C., B. B. Ferguson, and D. Mozzoni (2003), An $n = 90$ internal potential function of the Martian crustal magnetic field, *J. Geophys. Res.*, 108, 5008, doi:10.1029/2000JE001487.
- Crider, D. H., *et al.* (2002), Observations of the latitude dependence of the location of the Martian magnetic pileup boundary, *Geophys. Res. Lett.*, 29(8), 1170, doi:10.1029/2001GL013860.
- Crider, D. H., D. Vignes, A. M. Krymskii, T. K. Breus, N. F. Ness, D. L. Mitchell, J. A. Slavin, and M. H. Acuña (2003), A proxy for determining solar wind dynamic pressure at Mars using Mars Global Surveyor data, *J. Geophys. Res.*, 108, 1461, doi:10.1029/2003JA009875.
- Dubinin, E., *et al.* (2008), Plasma environment of Mars as observed by simultaneous MEX-ASPERA-3 and MEX-MARSIS observations, *J. Geophys. Res.*, 113, A10217, doi:10.1029/2008JA013355.
- Dubinin, E., M. Fraenz, J. Woch, F. Duru, D. Gurnett, R. Modolo, S. Barabash, and R. Lundin (2009), Ionospheric storms on Mars: Impact of the corotating interaction region, *Geophys. Res. Lett.*, 36, L01105, doi:10.1029/2008GL036559.
- Duru, F., D. A. Gurnett, T. F. Averkamp, D. L. Kirchner, R. L. Huff, A. M. Persoon, J. J. Plaut, and G. Picardi (2006), Magnetically controlled structures in the ionosphere of Mars, *J. Geophys. Res.*, 111, A12204, doi:10.1029/2006JA011975.
- Edberg, N. J. T., M. Lester, S. W. H. Cowley, and A. I. Eriksson (2008), Statistical analysis of the location of the Martian magnetic pileup boundary and bow shock and the influence of crustal magnetic fields, *J. Geophys. Res.*, 113, A08206, doi:10.1029/2008JA013096.

- Edberg, N. J. T., D. A. Brain, M. Lester, S. W. H. Cowley, R. Modolo, M. Fränz, and S. Barabash (2009), Plasma boundary variability at Mars as observed by Mars Global Surveyor and Mars Express, *Ann. Geophys.*, *27*, 3537–3550, doi:10.5194/angeo-27-3537-2009.
- Fillingim, M. O., L. M. Peticolas, R. J. Lillis, D. A. Brain, J. S. Halekas, D. L. Mitchell, R. P. Lin, D. Lummerzheim, S. W. Bougher, and D. L. Kirchner (2007), Model calculations of electron precipitation induced ionization patches on the nightside of Mars, *Geophys. Res. Lett.*, *34*, L12101, doi:10.1029/2007GL029986.
- Fränz, M., et al. (2006), Plasma intrusion above Mars crustal fields—Mars Express ASPERA-3 observations, *Icarus*, *182*, 406–412, doi:10.1016/j.icarus.2005.11.016.
- Fränz, M., E. Dubinin, E. Nielsen, J. Woch, S. Barabash, and R. Lundin (2010), Transterminator ion flow in the Martian ionosphere, *Planet. Space Sci.*, *58*(11), 1442–1454, doi:10.1016/j.pss.2010.06.009.
- Gurnett, D. A., D. L. Kirchner, R. L. Huff, D. D. Morgan, A. M. Persoon, F. Duru, E. Nielsen, A. Safaeinili, J. J. Plaut, and G. Picardi (2005), Radar soundings of the ionosphere of Mars, *Science*, *310*, 1929–1933, doi:10.1126/science.1121868.
- Haider, S. A., K. K. Mahajan, and E. Kallio (2011), Mars ionosphere: A review of experimental results and modeling studies, *Rev. Geophys.*, *49*, RG4001, doi:10.1029/2011RG000357.
- Krymskii, A. M., N. F. Ness, D. H. Crider, T. K. Breus, M. H. Acuña, and D. P. Hinson (2004), Solar wind interaction with the ionosphere/atmosphere and crustal magnetic fields at Mars: Mars Global Surveyor Magnetometer/Electron Reflectometer, radio science, and accelerometer data, *J. Geophys. Res.*, *109*, A11306, doi:10.1029/2004JA010420.
- Langlais, B., M. E. Purucker, and M. Mandea (2004), Crustal magnetic field of Mars, *J. Geophys. Res.*, *109*, E02008, doi:10.1029/2003JE002048.
- Lillis, R. J., and D. A. Brain (2013), Nightside electron precipitation at Mars: Geographic variability and dependence on solar wind conditions, *J. Geophys. Res. Atmos.*, *118*, 3546–3556, doi:10.1002/jgra.50171.
- Lillis, R. J., D. L. Mitchell, R. P. Lin, J. E. P. Connerney, and M. H. Acuña (2004), Mapping crustal magnetic fields at Mars using electron reflectometry, *Geophys. Res. Lett.*, *31*, L15702, doi:10.1029/2004GL020189.
- Lillis, R. J., H. V. Frey, M. Manga, D. L. Mitchell, R. P. Lin, M. H. Acuña, and S. W. Bougher (2008), An improved crustal magnetic field map of Mars from electron reflectometry: Highland volcano magmatic history and the end of the Martian dynamo, *Icarus*, *194*, 575–596, doi:10.1016/j.icarus.2007.09.032.
- Lillis, R. J., M. O. Fillingim, L. M. Peticolas, D. A. Brain, R. P. Lin, and S. W. Bougher (2009), Nightside ionosphere of Mars: Modeling the effects of crustal magnetic fields and electron pitch angle distributions on electron impact ionization, *J. Geophys. Res.*, *114*, E11009, doi:10.1029/2009JE003379.
- Lillis, R. J., M. E. Purucker, J. S. Halekas, K. L. Louzada, S. T. Stewart-Mukhopadhyay, M. Manga, and H. V. Frey (2010), Study of impact demagnetization at Mars using Monte Carlo modeling and multiple altitude data, *J. Geophys. Res.*, *115*, E07007, doi:10.1029/2009JE003556.
- Lillis, R. J., D. A. Brain, G. T. Delory, D. L. Mitchell, J. G. Luhmann, and R. P. Lin (2012), Evidence for superthermal secondary electrons produced by SEP ionization in the Martian atmosphere, *J. Geophys. Res.*, *117*, E03004, doi:10.1029/2011JE003932.
- Liu, H., H. Lühr, V. Henize, and W. Köhler (2005), Global distribution of the thermospheric total mass density derived from CHAMP, *J. Geophys. Res.*, *110*, A04301, doi:10.1029/2004JA010741.
- Lühr, H., M. Rother, W. Köhler, P. Ritter, and L. Grunwaldt (2004), Thermospheric up-welling in the cusp region: Evidence from CHAMP observations, *Geophys. Res. Lett.*, *31*, L06805, doi:10.1029/2003GL019314.
- Lundin, R., S. Barabash, M. Yamauchi, H. Nilsson, and D. Brain (2011), On the relation between plasma escape and the Martian crustal magnetic field, *Geophys. Res. Lett.*, *38*, L02102, doi:10.1029/2010GL046019.
- Morgan, D., O. Witasse, E. Nielsen, D. Gurnett, F. Duru, and D. Kirchner (2013), The processing of electron density profiles from the Mars Express MARSIS topside sounder, *Radio Sci.*, *48*(3), 197–207, doi:10.1002/rds.20023.
- Morgan, D. D., D. A. Gurnett, D. L. Kirchner, J. L. Fox, E. Nielsen, and J. J. Plaut (2008), Variation of the Martian ionospheric electron density from Mars Express radar soundings, *J. Geophys. Res.*, *113*, A09303, doi:10.1029/2008JA013313.
- Nagy, A. F., et al. (2004), The plasma environment of Mars, *Space Sci. Rev.*, *111*, 33–114, doi:10.1023/B:SPAC.0000032718.47512.92.
- Ness, N. F., M. H. Acuña, J. E. P. Connerney, A. J. Kliore, T. K. Breus, A. M. Krymskii, P. Cloutier, and S. J. Bauer (2000), Effects of magnetic anomalies discovered at Mars on the structure of the Martian ionosphere and solar wind interaction as follows from radio occultation experiments, *J. Geophys. Res.*, *105*, 15,991–16,004, doi:10.1029/1999JA000212.
- Nielsen, E., et al. (2007a), Local plasma processes and enhanced electron densities in the lower ionosphere in magnetic cusp regions on Mars, *Planet. Space Sci.*, *55*, 2164–2172, doi:10.1016/j.pss.2007.07.003.
- Nielsen, E., X.-D. Wang, D. A. Gurnett, D. L. Kirchner, R. Huff, R. Orosei, A. Safaeinili, J. J. Plaut, and G. Picardi (2007b), Vertical sheets of dense plasma in the topside Martian ionosphere, *J. Geophys. Res.*, *112*, E02003, doi:10.1029/2006JE002723.
- Nilsson, H., et al. (2006), Investigation of the influence of magnetic anomalies on ion distributions at Mars, *Space Sci. Rev.*, *126*, 355–372, doi:10.1007/s11214-006-9030-0.
- Nilsson, H., N. J. T. Edberg, G. Stenberg, S. Barabash, M. Holmström, Y. Futaana, R. Lundin, and A. Fedorov (2011), Heavy ion escape from Mars, influence from solar wind conditions and crustal magnetic fields, *Icarus*, *215*, 475–484, doi:10.1016/j.icarus.2011.08.003.
- Němec, F., D. D. Morgan, D. A. Gurnett, and F. Duru (2010), Nightside ionosphere of Mars: Radar soundings by the Mars Express spacecraft, *J. Geophys. Res.*, *115*, E12009, doi:10.1029/2010JE003663.
- Němec, F., D. D. Morgan, D. A. Gurnett, and D. A. Brain (2011), Areas of enhanced ionization in the deep nightside ionosphere of Mars, *J. Geophys. Res.*, *116*, E06006, doi:10.1029/2011JE003804.
- Opgenoorth, H. J., R. S. Dhillon, L. Rosenqvist, M. Lester, N. J. T. Edberg, S. E. Milan, P. Withers, and D. Brain (2010), Day-side ionospheric conductivities at Mars, *Planet. Space Sci.*, *58*, 1139–1151, doi:10.1016/j.pss.2010.04.004.
- Opgenoorth, H. J., D. J. Andrews, M. Fränz, M. Lester, N. J. T. Edberg, D. D. Morgan, F. Duru, O. Witasse, and A. O. Williams (2013), Mars ionospheric response to solar wind variability, *J. Geophys. Res. Space Physics*, *118*, 6558–6587, doi:10.1002/jgra.50537.
- Picardi, G., et al. (2004), MARSIS: Mars Advanced Radar for Subsurface and Ionosphere Sounding, in *Mars Express: The Scientific Payload*, vol. 1240, edited by A. Wilson and A. Chicarro, pp. 51–69, ESA Spec. Pub., Noordwijk, Neth.
- Purucker, M., D. Ravat, H. Frey, C. Voorhies, T. Sabaka, and M. Acuña (2000), An altitude-normalized magnetic map of Mars and its interpretation, *Geophys. Res. Lett.*, *27*, 2449–2452, doi:10.1029/2000GL000072.
- Sánchez-Cano, B., O. Witasse, M. Herraiz, S. M. Radicella, J. Bauer, P.-L. Blelly, and G. Rodríguez-Caderot (2012), Retrieval of ionospheric profiles from the Mars Express MARSIS experiment data and comparison with radio occultation data, *Geosci. Instrum. Method. Data Syst. Discuss.*, *1*, 77–84, doi:10.5194/gi-1-77-2012.
- Sánchez-Cano, B., S. Radicella, M. Herraiz, O. Witasse, and G. Rodríguez-Caderot (2013), NeMars: An empirical model of the Martian dayside ionosphere based on Mars Express MARSIS data, *Icarus*, *225*(1), 236–247, doi:10.1016/j.icarus.2013.03.021.

- Soobiah, Y., et al. (2006), Observations of magnetic anomaly signatures in Mars Express ASPERA-3 ELS data, *Icarus*, 182, 396–405, doi:10.1016/j.icarus.2005.10.034.
- Witasse, O., T. Cravens, M. Mendillo, J. Moses, A. Kliore, A. Nagy, and T. Breus (2008), Solar system ionospheres, *Space Sci. Rev.*, 139, 235–265, doi:10.1007/s11214-008-9395-3.
- Withers, P., M. Mendillo, H. Rishbeth, D. P. Hinson, and J. Arkani-Hamed (2005), Ionospheric characteristics above Martian crustal magnetic anomalies, *Geophys. Res. Lett.*, 32, L16204, doi:10.1029/2005GL023483.